International Journal of Engineering & Technology, 7 (4.10) (2018) 873-879

International Journal of Engineering & Technology

Website: www.sciencepubco.com/index.php/IJET

Research paper

Heat and Mass Transfer Effects on MHD Nanofluids Past Over an Inclined Plate

G. Palani[1], A.Arutchelvi[2,*]

[1.]Department of Mathematics, Dr. Ambedkar Govt. Arts College, Chennai 600039, Tamil Nadu, INDIA
[2] Department of Mathematics, Bharathi Women's College, Chennai 600108, Tamil Nadu, INDIA
**Corresponding author E-mail: aarutchelvi@gmail.com*

Abstract

This paper highlights the effects of radiation and MHD nanofluid flowing over a permeable medium that undergoes chemical reaction in first order. The nanoparticles used in the study are copper, aluminium oxide, titanium oxide and silver. The governing partial differential equations are solved by Laplace transform technique. The influences of several values of the physical parameters on velocity, temperature, concentration profiles are analyzed in an extensive way. The derived findings are depicted in graphs. The numerical results are found for Skin friction coefficient, Nusselt and Sherwood numbers that are revealed in tabular form.

Keywords: *natural convection; nanofluid; inclined plate; magnetic field*

1. Introduction

Choi [2] has introduced the Nanofluid. It is a nano-meter sized particle that is suspended in the base liquid. The purpose of the usage of nanoparticles in the base liquid is to enhance the heat transfer. Conventional fluids have relatively lesser thermal conductivity than the nanofluids. Solar collectors have shown the phenomenal conception of radiative heat transfer in nanofluids. In the recent years nanofluid transport in permeable medium is apt, that has come in to the limelight. Nanofluids transmits the metallic particle and plays a vital role in the various fields like, drug delivery, biomedical, industrial engineering, solar and power plant cooling, chemical processes by the simultaneous transmission of heat and mass diffusion. To substantiate the implementation of the nanoparticles, researchers have conducted various surveys

Anjali Devi and Suriyakumar [1] have perceived and dealt with the problem of the mixed convective hydro magnetic nonlinear nanofluid flow past an inclined plate. Das and Jana [4] examined the impacts of radiative transfer of heat in MHD convective flow past through a moving vertical plate. Das, Jana and Makinde [5] have explained the significance of a resourceful heat radiation through a vertical channel filled with nano fluids. Durga Prasad, Varma , KiranKumar [6] has thoroughly carried out an experiment on radiation absorption in MHD flow of nanofluid using small perturbation method. Geetha, Muthucumaraswamy, Sharmila [7] have examined the magneto hydrodynamic effects on a transient nanofluid past over a vertical plate. Jyotsna Rani Pattnaik,Suprava and Gouranga Charan Dash [8] have tested the outcome of mass transfer on MHD flow past via porous medium with radiation over an inclined plate. The area of heat transmission in nanofluids has been clearly elaborated by Das and Choi [3] and Wang and Mazumdar[14] in review articles. MHD natural convective nanofluid flow under the influence of radiation over a vertical plate was given by Loganath and, Nirmal Chand and Ganasan[9] using finite difference method. Ramana Reddya, Sugunammaa Sandeep and Sulochanab [10] used perturbation technique to study the impact of chemical transformation and emission of nanofluid gyrating over a permeable even plate. The unstable MHD heat transformation of nanofluid past over the vertical plate with the influence of variable temperature and thermal radiation.This method was analytically studied by Rajesh Vemula ,Lomenta Debnath and Sridevi Chakrala [11]. Sandeep† and Jagadeesh Kumar[12] considered Runge-Kutta integration scheme with shooting technique is to resolve the consequence of heat and mass transposition in nanofluid flow over an inclined sheet along with dust volume fraction of nanoparticles. An analysis has been carried out by Sandeep, Sulochana, RushiKumar [13] by using Runge–Kutta with shooting technique subject to MHD radiative flow and a dusty nanofluid of heat transfer over an exponentially enlarging surface.

2. Governing equations

An unsteady free convective flow of a viscid, incompressible nanofluid is sent over an inclined plate makes an inclination angle α to the vertical through penetrable medium in the presence of an applied MHD is considered. Let x and y represents axes along the plate and perpendicular to the plate respectively. In the beginning both the plate and nanofluid are set and maintained at the same temperature T_∞' and concentration C_∞'.At t≥0, the plate impulsively starts to move in its plane with velocity u_0. Simultaneously temperature and concentration levels close to the plate is to suddenly raised to T_w' and C_w' respectively. The strength of Magnetic field B_0 is enforced and positioned perpendicular to the flow, and

radiative heat flux q_r is described in energy equation. In dealing with this problem we further understand that both fluid and nanoparticles are in thermal equilibrium and act as single phase therefore no slip condition among them.

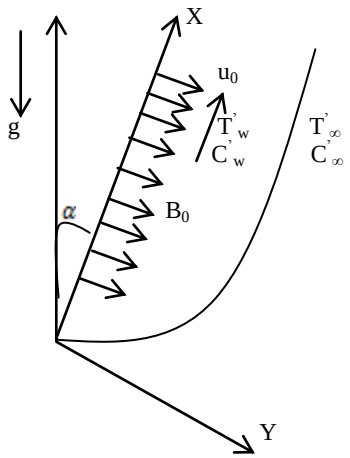

Figure 1: Flow geometry

Table 1: Thermophysical features of water and nanoparticles

Physical properties	Water	Cu	Al_2O_3	TiO_2	Ag
ρ(kg / m^3)	997.1	8933	3970	4250	10500
C_p (J / kgK)	4179	385	765	686.2	235
k(W /mK)	0.613	401	40	8.9538	429
ß x 10^5 (K^{-1})	21	1.67	0.85	0.90	1.89
σ(S / m)	5.5 x 10^{-6}	59.6 x 10^6	35 x 10^6	2.6 x 10^6	62.1x 10^6

The basic equations are formulated with the above stated assumptions:

$$\rho_{nf}\frac{\partial u'}{\partial t'} = g(\rho\beta_T)_{nf}(T'-T'_\infty)\cos\alpha + g(\rho\beta_C)_{nf}(C'-C'_\infty)\cos\alpha + \mu_{nf}\frac{\partial^2 u'}{\partial y'^2} - \sigma_{nf}B_0^{\,2}u' - \frac{\nu_f}{k'}u' \tag{1}$$

$$(\rho c_p)_{nf}\frac{\partial T'}{\partial t'} = k_{nf}\frac{\partial^2 T'}{\partial y'^2} - \frac{\partial q_r}{\partial y'} \tag{2}$$

$$\frac{\partial C'}{\partial t'} = D\frac{\partial^2 C'}{\partial y'^2} - k_l(C'-C_\infty') \tag{3}$$

Initial and boundary conditions are:

$$t'\le 0:\ u'=0,\quad T'=T'_\infty,\quad C'=C'_\infty,\quad \text{for all}\quad y'$$
$$t'>0:\ u'=u_0,\quad T'=T'_w,\quad C'=C'_w,\quad \text{at}\quad y'=0$$
$$u'\to 0\quad T'\to T'_\infty,\ C'\to C'_\infty\quad \text{as}\quad y'\to\infty \tag{4}$$

Where the following symbols $\mu_{nf}, \beta_{nf}, \rho_{nf}, k_{nf}$ and $(\rho c_p)_{nf}$, represent the effective dynamic viscosity, thermal expansion coefficient, density, thermal conductivity, and heat capacitance of the nanofluid respectively, which are given by

$$\mu_{nf} = \frac{\mu_f}{(1-\phi)^{2.5}}$$
$$\rho_{nf} = (1-\phi)\rho_f + \phi\rho_s$$
$$(\rho c_p)_{nf} = (1-\phi)(\rho c_p)_f + \phi(\rho c_p)_s,$$
$$(\rho\beta_T)_{nf} = (1-\phi)(\rho\beta_T)_f + \phi(\rho\beta_T)_s,$$
$$(\rho\beta_C)_{nf} = (1-\phi)(\rho\beta_C)_f + \phi(\rho\beta_C)_s,$$
$$\sigma_{nf} = \sigma_f\left[1+\frac{3(\sigma-1)\phi}{\sigma+2-(\sigma-1)\phi}\right]$$
$$\sigma = \frac{\sigma_s}{\sigma_f}$$
$$k_{nf} = k_f\left[\frac{k_s+2k_f-2\phi(k_f-k_s)}{k_s+2k_f+\phi(k_f-k_s)}\right] \tag{5}$$

where ϕ denotes the volume fraction of the nanoparticle. Here f, nf and s represents the basic fluid, thermophysical characteristic of nanoparticle and nano solid respectively.

Relevant dimensionless variables are

$$U=\frac{u'}{u_0},\ t=\frac{t'u_0^{\,2}}{\nu_f},\ Y=\frac{y'u_0}{\nu_f},\ M=\frac{B_0^{\,2}\sigma_f\nu_f}{\rho_f u_0^{\,2}},\ \theta=\frac{T'-T'_\infty}{T'_w-T'_\infty},\ \varphi=\frac{C'-C'_\infty}{C'_w-C'_\infty},$$
$$Grt=\frac{g\,\nu_f(\beta_T)_f(T'_w-T'_\infty)}{u_0^{\,3}},\ Grc=\frac{g\,\nu_f(\beta_C)_f(C'_w-C'_\infty)}{u_0^{\,3}},\ \Pr=\frac{(\mu c_p)_f}{k_f},$$
$$R=\frac{16\,a^*\sigma T'^{\,3}_\infty}{k_f}\left(\frac{\nu_f^{\,2}}{u_0^{\,2}}\right),\ S_c=\frac{\nu_f}{D},\ K=k_l\left(\frac{\nu_f}{u_0^{\,2}}\right),\ K_p=k'\rho_f\left(\frac{u_0^{\,2}}{\nu_f^{\,2}}\right) \tag{6}$$

To describe q_r Rosseland approximation is employed and it is given by $q_r=\frac{-4\sigma}{3k^*}\frac{\partial T^4}{\partial y}$

here σ and k*stand for are Stefan-Boltzmann constant and the mean absorption coefficient respectively.

$$\frac{\partial q_r}{\partial y} = -4a^*\sigma\left(T'^4_\infty - T'^4\right) \tag{7}$$

Taylor series method is applied to extend T'^4 about T'_∞

$$T'^4 \cong 4T'^3_\infty T' - 3T'^4_\infty \tag{8}$$

By using equations (6) and (7), equation (2) reduces to

$$(\rho c_p)_{nf}\frac{\partial T'}{\partial t'} = k_{nf}\frac{\partial^2 T'}{\partial y'^2} + 16a^*\sigma T'^3_\infty\,(T'_\infty - T') \tag{9}$$

By substituting equations (4) to (6) in (1), (9), and (3) yield the following equation,

$$x_1\frac{\partial U}{\partial t} = x_7\frac{\partial^2 U}{\partial Y^2} - x_4 MU + x_2 Grt\theta\cos\alpha + x_3 GrcC\cos\alpha - \frac{U}{K_P} \tag{10}$$

$$x_5\frac{\partial\theta}{\partial t} = \frac{x_6}{\Pr}\frac{\partial^2\theta}{\partial Y^2} - \frac{R}{\Pr}\theta \tag{11}$$

$$\frac{\partial C}{\partial t} = \frac{1}{Sc}\frac{\partial^2 C}{\partial Y^2} - KC \tag{12}$$

Where

$$x_1=(1-\phi)+\phi\left(\frac{\rho_s}{\rho_f}\right),\quad x_2=(1-\phi)+\phi\left(\frac{(\rho\beta_T)_s}{(\rho\beta_T)_f}\right),\quad x_3=(1-\phi)+\phi\left(\frac{(\rho\beta c)_s}{(\rho\beta_C)_f}\right),$$
$$x_4=\left(\frac{1+3(\sigma-1)\phi}{\sigma+2-(\sigma-1)\phi}\right),\ x_5=(1-\phi)+\phi\left(\frac{(\rho c_p)_s}{(\rho c_p)_f}\right),$$

$$x_6 = \left[\frac{k_s + 2k_f - 2\phi(k_f - k_s)}{k_s + 2k_f + \phi(k_f - k_s)}\right], \quad x_7 = \frac{1}{(1-\phi)^{2.5}} \tag{13}$$

Also R ,Pr and Gr refer to the radiation parameter, Prandtl number Grashof number. The corresponding non-dimensional forms are,

$$t \le 0 : U = 0,\ \theta = 0,\ C = 0 \quad for\ all \quad Y$$

$$t > 0 : U = 1,\ \theta = 1,\ C = 1 \quad at \quad Y = 0$$

$$U \to 0,\ \theta \to 0,\ C \to 0 \quad as \quad Y \to \infty \tag{14}$$

3. Solution Procedure

Equations from (10) to (12) are subjected to the conditions (14) using Laplace transform method and the results are given below.

$$\begin{aligned}
U = {} & \frac{1}{2}\left[\exp(2\eta\sqrt{R_3R_4t})\ erfc\left(\eta\sqrt{R_4} + \sqrt{R_3t}\right) + \exp(-2\eta\sqrt{R_3R_4t})\ erfc\left(\eta\sqrt{R}_4 - \sqrt{R_3t}\right)\right] + \\
& \frac{R_7}{2R_5}\left[\exp(2\eta\sqrt{R_3R_4t})\ erfc\left(\eta\sqrt{R_4} + \sqrt{R_3t}\right) + \exp(-2\eta\sqrt{R_3R_4t})\ erfc\left(\eta\sqrt{R}_4 - \sqrt{R_3t}\right)\right] - \\
& \frac{R_7\exp(R_5t)}{2R_5}\left[\begin{matrix}\exp(2\eta\sqrt{R_4(R_3+R_5)t})\ erfc\left(\eta\sqrt{R}_4 + \sqrt{(R_3+R_5)t}\right) + \\ \exp(-2\eta\sqrt{R_4(R_3+R_5)t})\ erfc\left(\eta\sqrt{R}_4 - \sqrt{(R_3+R_5)t}\right)\end{matrix}\right] \\
& + \frac{R_8}{2R_6}\left[\exp(2\eta\sqrt{R_3R_4t})\ erfc\left(\eta\sqrt{R}_4 + \sqrt{R_3t}\right) + \exp(-2\eta\sqrt{R_3R_4t})\ erfc\left(\eta\sqrt{R}_4 - \sqrt{R_3t}\right)\right] - \\
& \frac{R_8\exp(R_6t)}{2R_6}\left[\begin{matrix}\exp(2\eta\sqrt{R_4(R_3+R_6)t})\ erfc\left(\eta\sqrt{R}_4 + \sqrt{(R_3+R_6)t}\right) + \\ \exp(-2\eta\sqrt{R_4(R_3+R_6)t})\ erfc\left(\eta\sqrt{R}_4 - \sqrt{(R_3+R_6)t}\right)\end{matrix}\right] - \\
& \frac{R_7}{2R_5}\left[\exp(2\eta\sqrt{abt})\ erfc\left(\eta\sqrt{a} + \sqrt{bt}\right) + \exp(-2\eta\sqrt{abt})\ erfc\left(\eta\sqrt{a} - \sqrt{bt}\right)\right] + \\
& \frac{R_7\exp(R_5t)}{2R_5}\left[\begin{matrix}\exp(2\eta\sqrt{a(b+R_5)t})\ erfc\left(\eta\sqrt{a} + \sqrt{(b+R_5)t}\right) + \\ \exp(-2\eta\sqrt{a(b+R_5)t})\ erfc\left(\eta\sqrt{a} - \sqrt{(b+R_5)t}\right)\end{matrix}\right] - \\
& \frac{R_8}{2R_6}\left[\exp(2\eta\sqrt{KS_ct})\ erfc\left(\eta\sqrt{S_c} + \sqrt{Kt}\right) + \exp(-2\eta\sqrt{KS_ct})\ erfc\left(\eta\sqrt{S_c} - \sqrt{Kt}\right)\right] + \\
& \frac{R_8\exp(R_6t)}{2R_6}\left[\begin{matrix}\exp(2\eta\sqrt{S_c(K+R_6)t})\ erfc\left(\eta\sqrt{S_c} + \sqrt{(K+R_6)t}\right) + \\ \exp(-2\eta\sqrt{S_c(K+R_6)t})\ erfc\left(\eta\sqrt{S_c} - \sqrt{(K+R_6)t}\right)\end{matrix}\right]
\end{aligned} \tag{15}$$

$$\theta = \frac{1}{2}\left[\exp(2\eta\sqrt{abt})\ erfc\left(\eta\sqrt{a} + \sqrt{bt}\right) + \exp(-2\eta\sqrt{abt})\ erfc\left(\eta\sqrt{a} - \sqrt{bt}\right)\right] \tag{16}$$

$$C = \frac{1}{2}\left[\exp(2\eta\sqrt{KS_ct})\ erfc\left(\eta\sqrt{S_C} + \sqrt{Kt}\right) + \exp(-2\eta\sqrt{KS_ct})\ erfc\left(\eta\sqrt{S_C} - \sqrt{Kt}\right)\right] \tag{17}$$

Where

$$a = \frac{x_5\,\mathrm{Pr}}{x_6},\ b = \frac{R}{x_5\,\mathrm{Pr}},\ R_1 = R_4(s+R_3),\ R_2 = -R_4(s+R_3)$$

$$R_3 = \left(\frac{Mx_4 + \frac{1}{K_p}}{x_1}\right),\ R_4 = \frac{x_1}{x_7},\ R_5 = \left(\frac{Mx_4 + \frac{1}{K_p} - x_7ab}{x_7a - x_1}\right)$$

$$R_6 = \left(\frac{Mx_4 + \frac{1}{K_p} - x_7KS_c}{x_7Sc - x_1}\right),\ R_7 = \left(\frac{-x_2Gr\cos\gamma}{x_7a - x_1}\right),\ R_8 = \left(\frac{-x_3Gc\cos\gamma}{x_7Sc - x_1}\right)$$

$$erfc(x) = \frac{2}{\sqrt{\pi}}\int_x^\infty e^{-t^2}dt$$

$$C_f = \frac{\tau_w}{\rho_f u_0^{\ 2}},$$

$$N_u = \frac{xq_w}{k_f(T_w - T_\infty)},$$

$$Sh_x = \frac{xq_m}{D(T_w - T_\infty)}$$

The shear stress, heat flux and mass flux are given by

$$\tau_w = \mu_{nf}\left(\frac{\partial u}{\partial y}\right)_{\eta=0}$$

$$q_w = -k_{nf}\left(\frac{\partial T'}{\partial y}\right)_{\eta=0}$$

$$q_m = -\mu_{nf}\left(\frac{\partial C'}{\partial y}\right)_{\eta=0}$$

The local skin friction coefficient is given by

$$C_f = -\frac{1}{(1-\phi)^{2.5}}\left(\frac{\partial U}{\partial \eta}\right)_{\eta=0}$$

Where

$$\begin{aligned}
\left(\frac{\partial U}{\partial \eta}\right)_{\eta=0} = {} & \frac{1}{(1-\phi)^{2.5}}\left[\sqrt{R_3R_4t}\ (1 - erf\left(\sqrt{R_3t}\right) + (2/\sqrt{\pi})\sqrt{R_4}\exp(-R_3t) - \sqrt{R_3R_4t}\ (1 + erfc\left(\sqrt{R_3t}\right)\right] + \\
& \frac{R_7}{R_5}\left[\sqrt{R_3R_4t}\ (1 - erf\left(\sqrt{R_3t}\right) + (2/\sqrt{\pi})\sqrt{R_4}\exp(-R_3t) - \sqrt{R_3R_4t}\ (1 + erf\left(\sqrt{R_3t}\right)\right] - \\
& \frac{R_7\exp(R_5t)}{R_5}\left[\begin{matrix}\sqrt{R_4(R_3+R_5)t}\ (1 - erf\left(\sqrt{(R_3+R_5)t}\right) + (2/\sqrt{\pi})\sqrt{R_4}\exp(-(R_3+R_5)t) - \\ \sqrt{R_4(R_3+R_5)t}\ (1 + erf\left(\sqrt{(R_3+R_5)t}\right)\end{matrix}\right] \\
& + \frac{R_8}{R_6}\left[\sqrt{R_3R_4t}\ (1 - erf\left(\sqrt{R_3t}\right) + (2/\sqrt{\pi})\sqrt{R_4}\exp(-R_3t) - \sqrt{R_3R_4t}\ (1 + erf\left(\sqrt{R_3t}\right)\right] - \\
& \frac{R_8\exp(R_6t)}{R_6}\left[\begin{matrix}\sqrt{R_4(R_3+R_6)t}\ (1 - erf\left(\sqrt{(R_3+R_6)t}\right) + (2/\sqrt{\pi})\sqrt{R_4}\exp(-(R_3+R_6)t) - \\ \sqrt{R_4(R_3+R_6)t}\ (1 + erf\left(\sqrt{(R_3+R_6)t}\right)\end{matrix}\right] - \\
& \frac{R_7}{R_5}\left[\sqrt{abt}\ (1 - erf\left(\sqrt{bt}\right) + (2/\sqrt{\pi})\sqrt{a}\exp(-bt) - \sqrt{abt}\ (1 + erf\left(\sqrt{bt}\right)\right] + \\
& \frac{R_7\exp(R_5t)}{R_5}\left[\begin{matrix}\sqrt{a(b+R_5)t}\ (1 - erf\left(\sqrt{(b+R_5)t}\right) + (2/\sqrt{\pi})\sqrt{a}\exp(-(b+R_5)t - \\ \sqrt{a(b+R_5)t}\ (1 - erf\left(\sqrt{(b+R_5)t}\right)\end{matrix}\right] - \\
& \frac{R_8}{R_6}\left[\sqrt{KS_ct}\ (1 - erf\left(\sqrt{Kt}\right) + (2/\sqrt{\pi})\sqrt{Sc}\exp(-Kt) - \sqrt{KS_ct}\ (1 + erf\left(\sqrt{Kt}\right)\right] + \\
& \frac{R_8\exp(R_6t)}{R_6}\left[\begin{matrix}\sqrt{S_c(K+R_6t)}\ (1 - erf\left(\sqrt{(K+R_6)t}\right) + (2/\sqrt{\pi})\sqrt{Sc}\exp(-(K+R_6)t) - \\ \sqrt{S_c(K+R_6)t}\ (1 - erf\left(\sqrt{(K+R_6)t}\right)\end{matrix}\right]
\end{aligned} \tag{18}$$

The local Nusselt number is given by,

$$N_u = -\frac{k_{nf}}{k_f}\left(\frac{\partial \theta}{\partial \eta}\right)_{\eta=0},$$

where

$$\left(\frac{\partial \theta}{\partial \eta}\right)_{\eta=0} = \left[\sqrt{abt}\ (1 - erf\left(\sqrt{bt}\right) + (2/\sqrt{\pi})\sqrt{a}\exp(-bt) - \sqrt{abt}\ (1 + erf\left(\sqrt{bt}\right)\right] \tag{19}$$

The local Sherwood number is given by,

$$Sh_u = -\frac{k_{nf}}{k_f}\left(\frac{\partial C}{\partial \eta}\right)_{\eta=0},$$

where

$$\left(\frac{\partial C}{\partial \eta}\right)_{\eta=0} = \left[\sqrt{KSct}\ (1 - erf\left(\sqrt{Kt}\right) + (2/\sqrt{\pi})\sqrt{Sc}\exp(-Kt) - \sqrt{KSct}\ (1 + erf\left(\sqrt{Kt}\right)\right] \tag{20}$$

4. Results and discussion

Numerical computations have been obtained from several factors that define the aspects of flow and the findings are demonstrated in the following graph. In the entire study several parameter Pr=0.71,Sc=0.6,R=0.5,t=0.5,Gr=5,Gc=10,Kp=0.2,ϕ=0.3,$\alpha=60^0$, M=3, K=0.1 are kept as constant except the variation in the corresponding figures and table

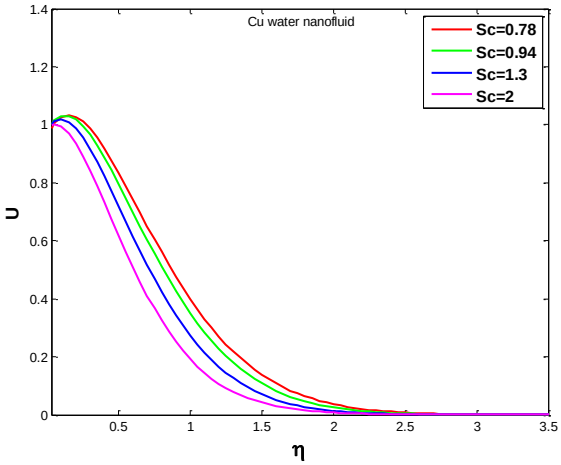

Fig.1: Variation of U with Sc

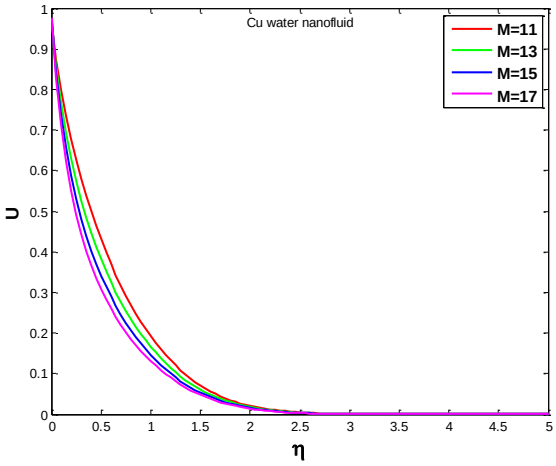

Fig.2: Variation of U with M

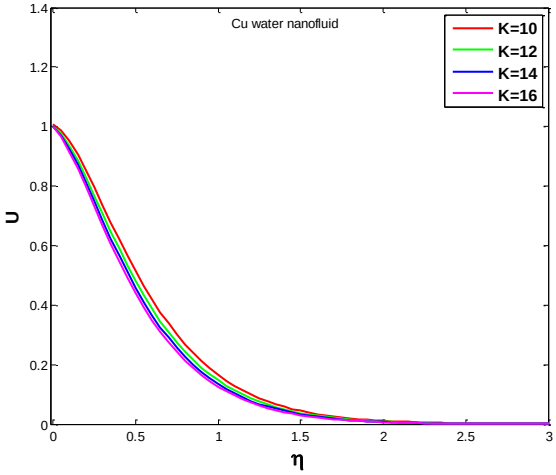

Fig.3: Variation of U with K

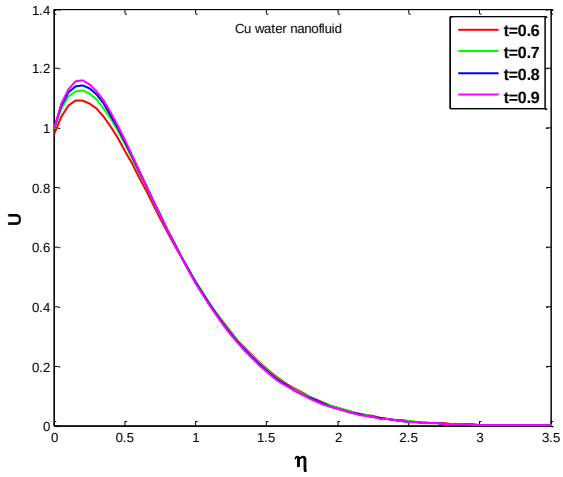

Fig.4: Variation of U with t

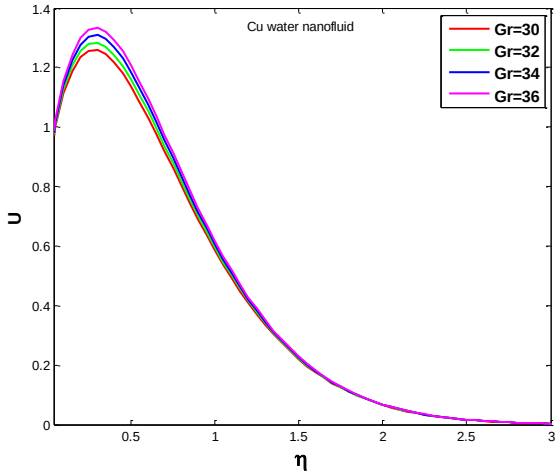

Fig.5: Variation of U with Gr

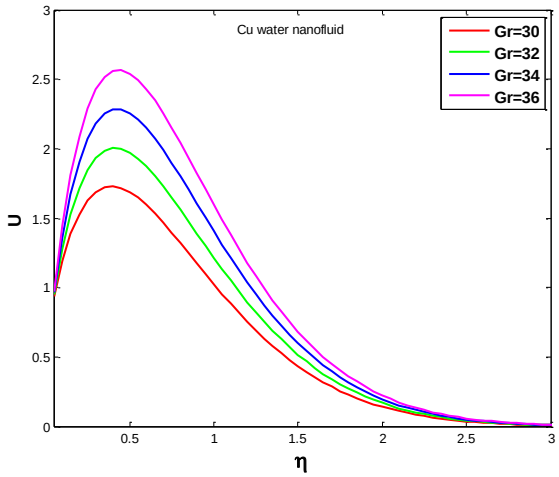

Fig.6: Variation of U with Gc

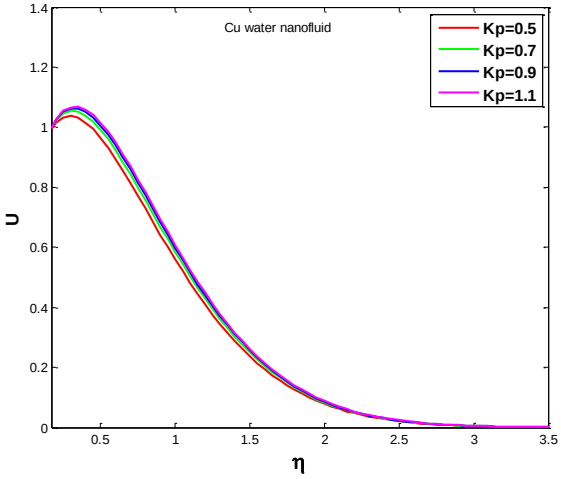

Fig.7: Variation of U with Kp

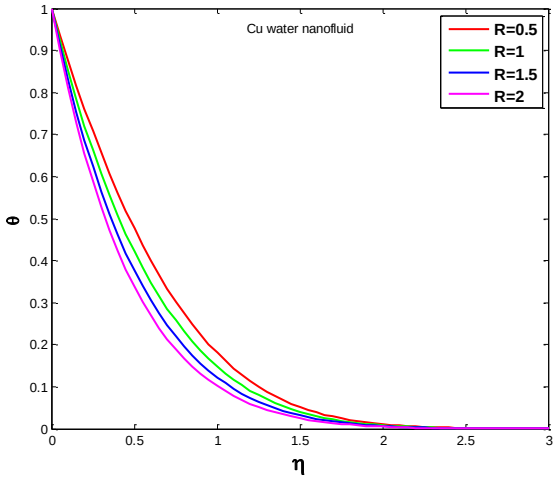

Fig.8: Variation of θ with R

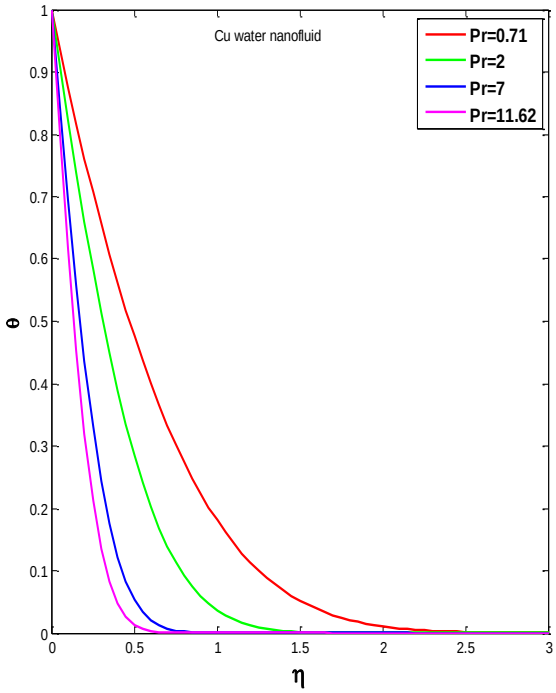

Fig.9: Variation of θ with Pr

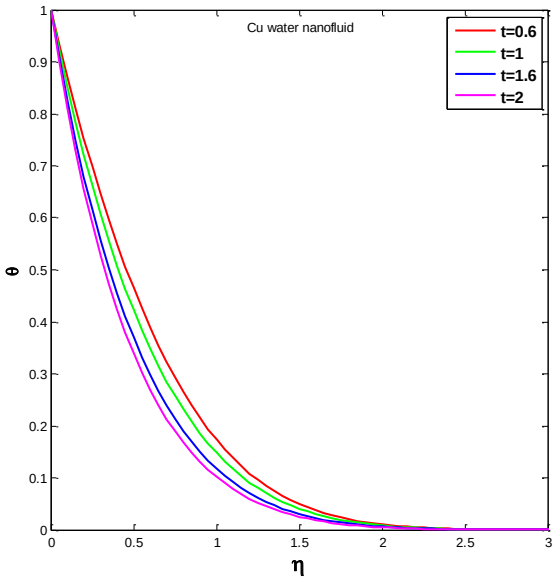

Fig.10: Variation of θ with t

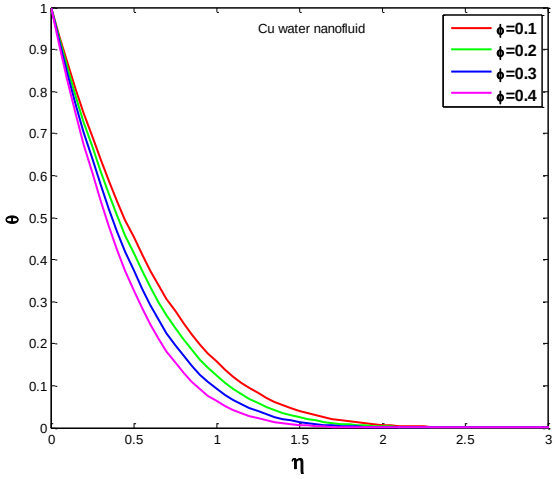

Fig.11: Variation of θ with ϕ

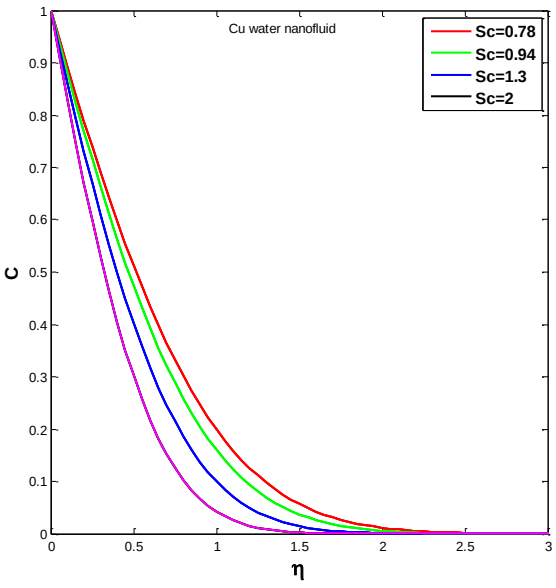

Fig.12: Variation of C with Sc

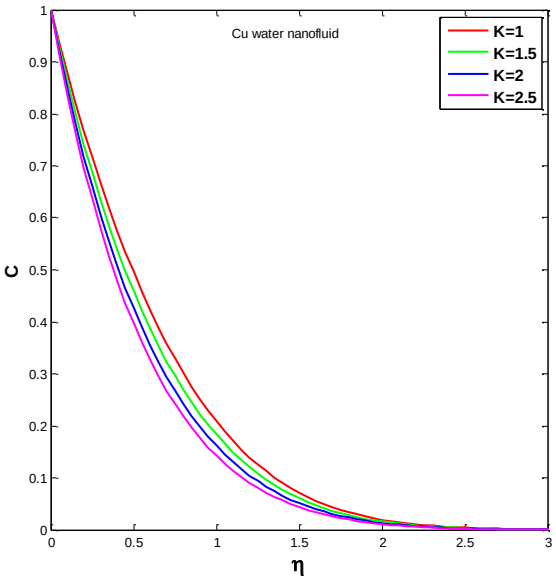

Fig.13: Variation of C with K

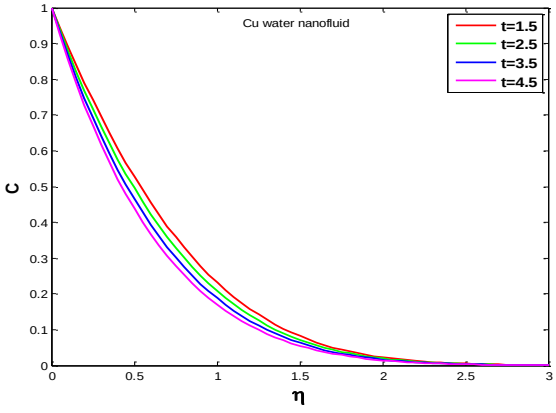

Fig.14: Variation of C with t

Fig 1.shows the consequences of Schmidt number on the velocity profile leads to the reduction with the raise of values in Sc.In fig 2. velocity boundary layer profile depicts contrastive values of magnetic parameter M, it shows the decreasing in velocity with the increasing values of magnetic field which tends to minimize the thickness of momentum borderline. The outcome of chemical reaction parameter on the velocity profile tends to decreases as K upsurge illustrated in Fig .3. Fig 4. shows the velocity of the fluid slowdowns when there is decrease in time. Figures 5. and 6. evidently prove the boundary layer thickness increases with the increasing values of Grashof number and mass Grashof number respectively. Fig 7. demonstrates the effect of penetrability factor Kp, as Kp increases, it reduces the drag force and therefore raises the velocity.

The result of radiation parameter on the temperature distribution drops down with the progressive values of R is plotted in Fig 8. In fig 9. the temperature profile shows the results of fluid temperature declines as Pr increases, because of the greater Prandtl number. This has comparatively performed low thermal conductivity which reduces the conduction and it results in dips down in the temperature. Fig 10. exhibits the variation of t on the temperature outline display that the temperature declines with the increasing values of t. In fig11. the temperature of the liquid falls by an increasing value of φ.

Fig 12. highlight the impact of Sc on concentration outline shows that the increase of Sc causes the decrease in concentration. Fig13. illustrates the chemical reaction factor results in the concentration profiles. It is accurate from the figure that an increase in K causes the gradual decrease in the concentration. Fig 14. reveals that increase of time causes the decrease of concentration profiles.

Table 2: Impact of different factors on skin friction coefficients for copper water nanofluid. Here K=0.2,α=45°,ϕ=0.2,Kp=3

Pr	Sc	t	Gr	Gc	C_f
0.71	0.16	0.5	5	5	32.2498
0.71	0.6	0.5	5	5	-2.2312
0.71	1.3	0.5	5	5	-22.3715
0.71	2.01	0.5	5	5	-40.1190
7	0.16	0.5	5	5	0.2540
7	0.6	0.2	5	5	-5.2142
7	1.3	0.5	5	5	-7.6329
7	2.01	0.5	5	5	-9.0902
0.71	0.6	0.2	5	5	-0.8656
0.71	0.6	0.6	5	5	0.6655
0.71	0.6	1.0	5	5	53.2496
0.71	0.6	0.5	10	5	0.3269
0.71	0.6	0.5	15	5	2.8851
0.71	0.6	0.5	5	10	-42.8663
0.71	0.6	0.5	5	15	-83.5014

It is noted from the table 2 the skin friction quantity reduces with the set-up values of Sc for Pr=0.71 and Pr=7. The increase in both time and thermal Grashof number steadily gear up the skin friction. . It also declines with the effect of raising values of mass Grashof number.

Computations of local Nusselt number:

Table 3.1: Variation of Nusselt number with nanoparticle volume fraction

	Nanoparticles			
Φ	**Cu**	**Al_2O_3**	**TiO_2**	**Ag**
0.01	-0.0713	-0.0726	-0.0731	-0.0751
0.02	-0.0724	-0.0750	-0.0760	-0.0800
0.03	-0.0735	-0.0774	-0.0788	-0.0847
0.04	-0.0746	-0.0797	-0.0816	-0.0894
0.05	-0.0757	-0.0819	-0.0843	-0.0939

Table 3.2: Variation of Nusselt number with radiation parameter

	Nanoparticles			
R	**Cu**	**Al_2O_3**	**TiO_2**	**Ag**
1	0.5484	0.5362	0.5348	0.5097
3	2.0607	2.0558	2.0653	2.0359
5	2.8746	2.8760	2.8922	2.8644
7	3.4511	3.4555	3.4760	3.4474
9	3.9252	3.9312	3.9549	3.9239

Table 3.3: Variation of Nusselt number with Prandl number

	Nanoparticles			
Pr	**Cu**	**Al_2O_3**	**TiO_2**	**Ag**
0.71	-0.0806	-0.0925	-0.0972	-0.1150
2	-0.9703	-0.9873	-0.9987	-1.0156
7	-2.5051	-2.5332	-2.5571	-2.5759
11.6	-3.3712	-3.4066	-3.4379	-3.4592
100	-10.4838	-10.5843	-10.6780	-10.7293

Table 3.4: Variation of Nusselt number with time

	Nanoparticles			
t	**Cu**	**Al_2O_3**	**TiO_2**	**Ag**
0.2	-0.5407	-0.5510	-0.5576	-0.5683
0.4	-0.2262	-0.2376	-0.2430	-0.2588
0.6	0.0578	0.0457	0.0416	0.0219
0.8	0.3149	0.t3026	0.2999	0.2771
1	0.5484	0.5362	0.5348	0.5097

The values obtained in table 3 reflects that the Nusselt number boost due to with the increasing values of radiation and time parameters however it declines with the growing values of volume fraction and prandl number .

Computations of local Sherwood number are shown in Table. 4

Table 4.1: Variation of Sherwood number with nanoparticle volume fraction

Nanoparticles				
Φ	**Cu**	**Al_2O_3**	**TiO_3**	Ag
0.1	-0.2507	-0.2515	-0.2546	-0.2507
0.2	-0.2128	-0.2143	-0.2199	-0.2128
0.3	-0.1782	-0.1803	-0.1880	-0.1782
0.4	-0.1465	-0.1490	-0.1585	-0.1465
0.5	-0.1173	-0.1202	-0.1312	-0.1173

Table 4.2: Variation of Sherwood number with Schmidt number

Nanoparticles				
Sc	**Cu**	**Al_2O_3**	**TiO_3**	**Ag**
0.6	-0.2507	-0.2515	-0.2546	-0.2507
0.96	-0.3171	-0.3182	-0.3220	-0.3171
1.22	-0.3575	-0.3587	-0.3630	-0.3575
1.3	-0.3690	-0.3702	-0.3747	-0.3690
1.60	-0.4094	-0.4107	-0.4157	-0.4094

Table 4.3: Variation of Sherwood number with chemical reac tion parameter

Nanoparticles				
K	**Cu**	**Al_2O_3**	**TiO_3**	**Ag**
0.2	-0.2507	-0.2515	-0.2546	-0.2507
0.4	0.1047	0.1050	0.1063	0.1047
0.6	0.4212	0.4225	0.4277	0.4211
0.8	0.7101	0.7124	0.7211	0.7101
1	0.9768	0.9800	0.9919	0.9768

Table 4.4: Variation of Sherwood number with time

	Nanoparticles			
t	**Cu**	**$Al_2 O_3$**	**TiO_3**	**Ag**
1	0.1047	0.1050	0.1050	0.1047
2	0.7101	0.7124	0.7211	0.7101
3	1.2246	1.2286	1.2436	1.2246
4	1.6725	1.6779	1.6983	1.6724
5	2.0675	2.0743	2.0995	2.0675

It is evident from the table 4 predominantly shows the decline of Sherwood number is due the increasing value of Φ but it increases with the raising values of K, time and Schmidt number

5. Conclusion

The effects of M, R, Φ, Kp, Sc, t and Pr over the flow field are shown by means of graphs.
The main findings are summarized as follows:
Fluid velocity reduces with the growing value of Schmidt number, magnetic field and chemical transformation in the boundary layer region but it increases with the increasing values of time, porous medium, thermal and mass Grashof number.
The temperature obtained in the boundary layer region drops down with the increasing values of radiation parameter, Prandtl number, time and nanoparticle volume fraction.
The species concentration drops-down with the increasing values of Schmidt number, chemical transmission parameter and time.

References

[1] S.P.Anjali Devi and P. Suriyakumar (2013), Numerical investigation of mixed convective hydro magnetic nonlinear nanofluid past an inclined plate, AIP Conference Proceedings, 1557, 281 - 285.

[2] S.U.S Choi (1995), Enhancing thermal conductivity of fluids with nanoparticles. In Developments and Applications of Non-Newtonian Flows.FED-Vol. 231/MD-Vol.66 pp99–105.American Society of Mechanical Engineers

[3] S.K. Das, S.U. Choi (2009), A review of heat transfer in nanofluids, Adv. Heat Transfer 46 119.

[4] S Das and R.N Jana (2015), Natural convective magneto nano fluid flow and radiative heat transfer past a moving vertical plate, Alexandria Eng. J, 54, 55 – 64.

[5] S Das, R.N Jana and O.D Makinde (2016), Transient Natural Convection in a Vertical Channel Filled with Nanofluids in the Presence of Thermal Radiation, Alexandria Engineering Journal, 55, 253 - 262.

[6] Durga Prasad, R.V.M.S.S. Kiran Kumar, S.V.K. Varma Heat and mass transfer analysis for the MHD flow of nanofluid with radiation absorption Ain Shams Engineering Journal (2016)

[7] E.Geetha,R.Sharmila,R.Muthucumaraswamy(2017) Magneto Hydrodynamic effects on a transient nanofluid past over an vertical plate International Journal of Materials Science ISSN 0973-4589 Volume 12, Number 2

[8] Jyotsna Rani Pattnaik , Gouranga Charan Dash , Suprava Singh, (2015): Radiation and mass transfer effects on MHD flow through porous medium past an exponentially accelerated inclined plate with variable temperature.A in Shams Engineering Journal.

[9] P Loganathan, P Nirmala Chand, P Ganesan(2015), Radiation effects on an unsteady MHD natural convective flow of a nanofluid past a vertical plate, Therm Sci, 19, 1037 - 509]

[10] J.V. Ramana Reddya, V. Sugunammaa, B. N. Sandeep, and C. Sulochanab (2016), Influence of chemical reaction, radiation and rotation on MHD nanofluid flow past a permeable flat plate in porous medium, Journal of the Nigerian Mathematical Society, 35, 48 – 65.

[11] Rajesh Vemula, Lokenath Debnath, Sridevi Chakrala, (2016),Unsteady MHD Free Convection Flow of Nanofluid Past an Accelerated Vertical Plate with Variable Temperature and Thermal Radiation, Int. J. Appl. Comput. Math, DOI 10.1007/s40819-016-0176-5.

[12] N. Sandeep† and M. S. Jagadeesh Kumar (2016), Heat and Mass Transfer in Nanofluid Flow over an Inclined Stretching Sheet with Volume Fraction ofDust and NanoparticlesJournal of Applied Fluid Mechanics, Vol. 9, No. 5, pp. 2205-2215.

[13] N. Sandeep a, C. Sulochana a, B. Rushi Kumar b (2016), Unsteady MHD radiative flow and heat transfer of a dusty nanofluid over an exponentially stretching surface, Engineering Science and Technology, an International Journal 19, 227–240

[14] X.Q. Wang, A.S. Mazumdar (2007), Heat transfer characteristics of nanofluids: a review, Int. J. Therm. Sci. 46, 119